

Spatio-attentive Graphs for Human–Object Interaction Detection

Frederic Z. Zhang Dylan Campbell Stephen Gould
 Australian National University
 {firstname.lastname}@anu.edu.au

Abstract

We address the problem of detecting human–object interactions in images using graphical neural networks. Our network constructs a bipartite graph of nodes representing detected humans and objects, wherein messages passed between the nodes encode relative spatial and appearance information. Unlike existing approaches that separate appearance and spatial features, our method fuses these two cues within a single graphical model allowing information conditioned on both modalities to influence the prediction of interactions with neighboring nodes. Through extensive experimentation we demonstrate the advantages of fusing relative spatial information with appearance features in the computation of adjacency structure, message passing and the ultimate refined graph features. On the popular HICO-DET benchmark dataset, our model outperforms state-of-the-art with an mAP of 27.18, a 10% relative improvement. Code has been made available. ¹

1. Introduction

The task of detecting human–object interactions (HOIs) requires localising and describing pairs of interacting humans and objects. In particular, an HOI is defined as a (subject, predicate, object) triplet, following the definition of visual relations from Lu et al. [20], where the subject and object are typically represented as labeled bounding boxes. For HOI triplets, the subject is always a human, and so the interactions of interest simplify to pairs of predicates and objects, e.g., *riding a horse* or *sitting on a bench*.

Since the output representations are inherently similar, HOI detection is most often approached as a downstream task of object detection. Given a set of object detections from an image, one may construct candidate human–object pairs by matching up the detected human and object instances exhaustively. Indeed, the vast majority of previous works [3, 7, 10, 15, 22, 21, 25, 6, 11] use an off-the-shelf object detector [23] as a preprocessing stage. We take the

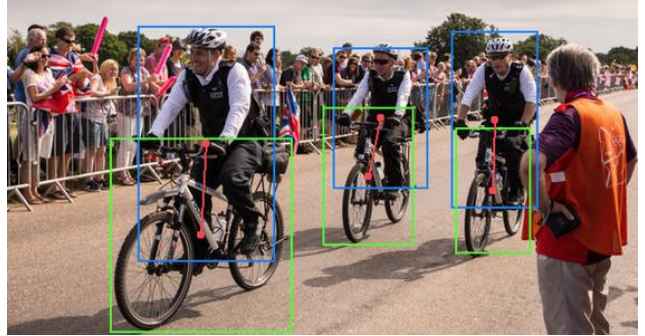


Figure 1. Many images contain far more non-interactive human–object pairs than interactive ones. In this example, which has only one type of interaction (riding a bike), there are many human–bike pairs but only three that are directly interactive. Correct inference of the interaction type and the correspondences requires a combination of appearance and spatial information to ensure that non-interactive pairs are suppressed.

same approach, leveraging the success of modern object detectors. While this converts the HOI detection task into the simpler HOI recognition task on a set of candidate human–object pairs, it is still far from being solved.

Recognising HOIs is extremely challenging. While image recognition discriminates between scene types [30] or prominent object types [24], focusing on the holistic understanding of an image, HOI recognition requires an understanding of the interactions between specific humans and objects at a much finer level. This requires reasoning about the subtle relationships between the instances as well as their contexts. This is particularly necessary when there are multiple human–object pairs with the same interaction type, where the model needs to correctly infer the interaction type and the correspondences between the individual instances. An example of this is shown in Fig. 1, where both spatial and appearance information is crucial to infer the HOI triplets and suppress the non-interactive pairs. In addition, many interactions do not have strong visual cues and can be quite abstract, such as *buying an apple* or *inspecting a boat*. This poses a big challenge for standard CNNs, which excel at recognising physical qualities such as texture and shape. However, HOI detection demands a

¹<https://github.com/fredzzhang/spatio-attentive-graphs>

more sophisticated architecture capable of performing logical reasoning, and distinguishing between visually similar interactions such as *boarding an airplane* and *exiting an airplane*, not merely recognising the visual cues of the humans and objects of interest. The complexity and ambiguity of the problem is such that even humans can fail to correctly recognize HOIs in images, despite our ability to reason about visual cues and spatial relationships. Following prior work, we make use of graphical models to better model these interrelationships and perform structured prediction.

Since humans and objects in an image play different roles in the interactions, we build a bipartite graph to characterize these interrelationships, wherein each human node is connected to each object node. As is intuitive, we use appearance features for a detected instance as the node encoding, be it a person or an object. The appearance features within the node’s bounding box are extracted using RoIAlign [12] from an off-the-shelf object detector [23]. However, edge encodings have been under-utilized in the HOI detection problem and offer the opportunity to modulate the appearance features with other useful pairwise information.

Let us consider the example shown in Fig. 1. Graphical models allow the propagation of contextual information between nodes. In this instance, each human node will receive information suggesting the presence of bikes, and so the predicted probability of *riding a bike* is increased. In previous work the message sent from a single bike node to all human nodes is identical, with the sole variable being a learnable weight that characterizes the connectivity or interactiveness [15]. This results in a high confidence on bike-related interactions for the most prominent human instances in the image. However, it cannot easily distinguish between nine putative human–bike pairs for the three most prominent humans. To address this drawback, we contend that it is crucial to incorporate spatial information to regulate the message passing procedure. To this end, we propose to use the spatial relationships between nodes as a form of attention on the messages, to modulate the appearance features with information about the spatial relationships and to attenuate the connectivity of pairs that are less probable to support an interaction.

Our primary contribution is a spatio-attentive graphical neural network for HOI detection with novel anisotropic messages passed between nodes of a bipartite graph, allowing the spatial relationships to regulate the propagation of contextual information. Spatial attention is also used to inform the classifier and the graph connectivity or interactiveness of the nodes. Unlike previous bipartite-graph-based methods for this task, we also demonstrate that our network benefits from the message passing iterations. We obtain state-of-the-art results on the challenging HICO-DET dataset [3], establishing a new benchmark for detecting

human–object interactions.

2. Related Work

The HOI detection pipeline has significant overlap with that of object detection. Analogous to two-stage object detectors, a common approach is to first generate human–object pair proposals and then classify their interactions. Specifically, Faster R-CNN [23] has been used in many preceding works [3, 7, 10, 15, 22, 21, 25, 6, 11] to generate objects, each of which is associated with a predicted class and a confidence score. Afterwards, with appropriate filtering, human–object pairs are constructed exhaustively from the remaining detections, that is, each human instance will be paired up with each object instance once. The rest of the pipeline varies, but typically employs a multi-branch structure to exploit different modalities of information. For instance, Chao et al. [3] proposed a three-branch architecture to process the human and object appearance features and their pairwise spatial relationships. Differently to many previous works, Liao et al. [16] presented a proposal-free HOI detection pipeline, where interactions are directly detected as keypoints. Such a keypoint represents the centre of the minimum covering rectangle for a human-object pair engaged in the predicted interaction. Positions of the human and object instances are obtained by regressing the displacements with respect to the detected interaction keypoint, similar to CornerNet [14], a keypoint-based object detector. Instead, we adopt the ubiquitous approach of using an off-the-shelf detector, due to their high performance and stability, and focus on improving the classification performance given a set of detections.

The choice of features has undergone significant development in recent research on HOI detection. Chao et al. [3] used RoIPool [8] to extract human and object appearance features and handcrafted a two-channel binary mask to encode the pairwise spatial relationships. While RoIAlign [12] is now used in preference to RoIPool for appearance feature extraction, the binary mask is still widely used [7, 6, 15, 25, 11]. However, Gupta et al. [10] argued that a handcrafted spatial feature is a more effective way to encode the spatial relationships, explicitly exposing the coordinates of the bounding box pairs, the intersection over union, the aspect ratios, etc. They and others [15, 31, 27] also proposed the use of human pose as additional information, although not all of the works demonstrated a clear benefit to using this side information. We observe similar benefits to using handcrafted spatial encodings, but do not make use of human pose information in this work. Instead, we focus on showing how structured architectures can best exploit appearance and spatial information to disambiguate human–object interactions.

Graphical models were introduced to HOI detection by Qi et al. [22]. They proposed a fully-connected graph

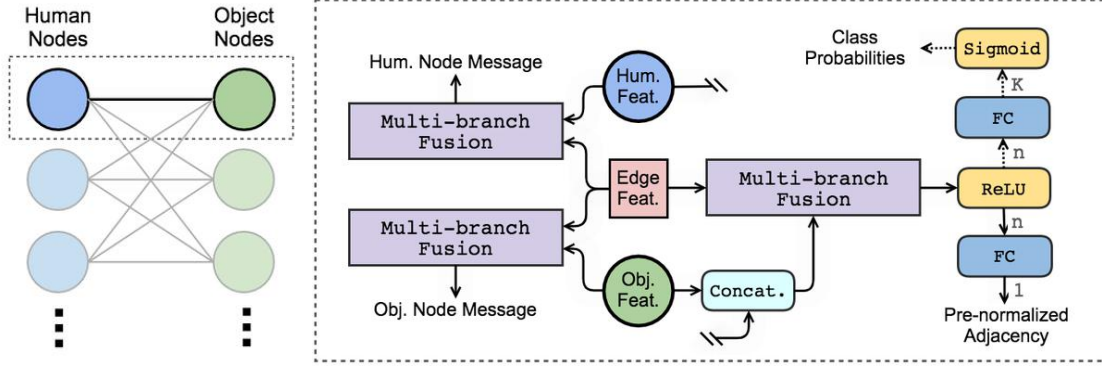


Figure 2. Diagram of our proposed bipartite graph and message passing algorithm. The graph structure and its connectivity is shown on the left. On the right, we zoom in on a particular pair of nodes and illustrate the message passing process. Messages are computed using the proposed multi-branch fusion, which takes as input the node encodings of the sender and the pairwise spatial features between the sending and the receiving nodes. To compute the adjacency between a node pair, we employ another multi-branch fusion module, which takes as input the concatenated node encodings and their pairwise spatial features. The output of is fed into an activation function (ReLU) and a linear layer to generate the adjacency value (pre-softmax). Upon finishing message passing, predicted scores for N target classes are computed using the same fusion module. The output dimension is displayed on each FC layer.

with detected human and object instances as nodes. The node features are initialized with box appearance features and iteratively updated with a message passing algorithm. Wang et al. [11] argued that the graph should take into consideration the fact that there are two sets of heterogeneous nodes, that is, the human nodes and object nodes. Thus, message passing between homogeneous nodes (intra-class messages) should be modeled differently from that between heterogeneous nodes (inter-class messages). Zhou et al. [31] proposed to model human parts (keypoints) as nodes and constructed star graphs using the detected keypoints, one type with the human as the centre node and another type with the object as the center node. Gao et al. [6] also took advantage of separate human-centric and object-centric graphs. They modeled human-object pairs as nodes, and employed the pairwise spatial relationships as node encodings. Lastly, Ulutan et al. [25] proposed a bipartite graph in addition to a visual branch, which makes use of the appearance features of human-object pairs and the global scene. Despite the success of their entire model, our testing indicates that their bipartite graph by itself performs considerably worse when more than one iteration of message passing is used. We conjecture that this is because the adjacency values are not properly normalized, resulting in node encodings that are dominated by the incoming messages. In contrast, our message passing algorithm does not demonstrate this behavior and is more stable. Moreover, our graphical model uses spatial relationship cues as well as appearance features to reason about interactions, allowing the message passing algorithm to disambiguate between visually similar but spatially distinct interactions. Overall, despite the suitability of graphical models for solving the HOI detection task, most previous work fails to exploit spa-

tial relationship information within the graph.

3. Spatio-attentive Graphs

To reason jointly about the appearance and spatial information of an image, we propose a graph neural network for detecting human-object interactions. The structure of the graph is shown in Figure 2. To obtain an initial set of detections $\{d_i\}_{i=1}^n$ for each image, we run an off-the-shelf object detector and apply appropriate filtering. We use Faster R-CNN [23], although our model is detector agnostic. The detections are given by the tuple $d_i = (\mathbf{b}_i, s_i, c_i)$, with bounding box coordinates $\mathbf{b}_i \in \mathbb{R}^4$, confidence score $s_i \in [0, 1]$ and predicted object class $c_i \in \mathcal{K}$, where \mathcal{K} is the set of object categories.

3.1. Bipartite Graph

We denote the bipartite graph as $\mathcal{G} = (\mathcal{H}, \mathcal{O}, \mathcal{E})$, where $\mathcal{H} = \{d_i \mid c_i = \text{"person"}\}$, $\mathcal{O} = \{d_i \mid c_i \neq \text{"person"}\}$, and \mathcal{E} is the set of edges, such that all vertices on one side of the bipartition are densely connected to those on the other. The node encodings are initialized with appearance features extracted using RoIAlign [12], and the edge encodings are computed as handcrafted feature vectors. We start by encoding the rudimentary spatial information: centre coordinates of the bounding boxes, widths, heights, aspect ratios and areas, all normalized by the corresponding dimension of the image. To characterize the pairwise relationships, we also include the intersection over union, the area of the human box normalized by that of the object box, and a directional encoding given by

$$[\text{ReLU}(d_x) \quad \text{ReLU}(-d_x) \quad \text{ReLU}(d_y) \quad \text{ReLU}(-d_y)], \quad (1)$$

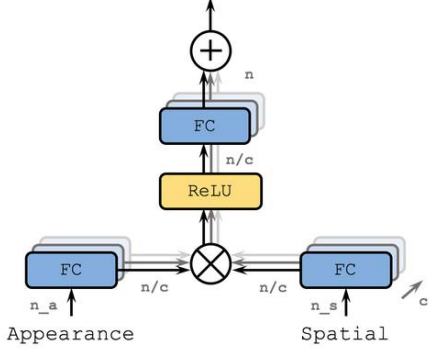


Figure 3. Structure of the multi-branch fusion module. The appearance and spatial features are mapped to c embedding spaces, fused with an elementwise product and then mapped to a fixed representation size. Outputs amongst different branches are aggregated by taking the sum. The input and output dimensions of each FC layer are shown in diagram.

where d_x and d_y are the differences between centre coordinates of the human and object boxes normalized by the dimensions of the human box. This gives us the pairwise spatial encoding $\tilde{\mathbf{p}} \in \mathbb{R}_+^{18}$. Following the practice of Gupta et al. [10], we concatenate the spatial encoding with its logarithm, allowing the network to learn second and higher order combinations of different terms. For numerical stability, a small constant $\epsilon > 0$ is added before taking the log, so

$$\mathbf{p} = \tilde{\mathbf{p}} \oplus \log(\tilde{\mathbf{p}} + \epsilon). \quad (2)$$

Denote node indices in the bipartition as $i \in \{1, \dots, |\mathcal{H}|\}$, $j \in \{1, \dots, |\mathcal{O}|\}$ and the time step as t . At initialization, appearance features are mapped to a lower dimension with a multilayer perceptron (MLP), populating the human and object node encodings, $\mathbf{x}_i^0, \mathbf{y}_j^0 \in \mathbb{R}^n$, correspondingly. Similarly, the edge encoding $\mathbf{z}_{ij} \in \mathbb{R}^n$ is obtained by mapping the pairwise spatial encoding to the same dimension using another MLP. The edge encodings are constant during message passing. We define our bi-directional message passing updates as

$$\mathbf{x}_i^{t+1} = \text{LN} \left(\mathbf{x}_i^t + \sigma \left(\sum_{j=1}^{|\mathcal{O}|} \alpha_{ij} M_{\mathcal{O} \rightarrow \mathcal{H}}(\mathbf{y}_j^t, \mathbf{z}_{ij}) \right) \right) \quad (3)$$

$$\mathbf{y}_j^{t+1} = \text{LN} \left(\mathbf{y}_j^t + \sigma \left(\sum_{i=1}^{|\mathcal{H}|} \alpha_{ji} M_{\mathcal{H} \rightarrow \mathcal{O}}(\mathbf{x}_i^t, \mathbf{z}_{ij}) \right) \right), \quad (4)$$

where LN denotes the LayerNorm operation [1], σ is the activation function (ReLU) and α is an (adjacency) weight between nodes. The message function M is different in each direction, as described below.

3.2. Multi-Branch Fusion

To exploit the appearance and spatial features jointly, we employ linear layers to map them to the same embedding space and take an elementwise product, which can be viewed as a form of (unnormalized) attention. Motivated by transformation cardinality explored in ResNeXt [29] and multi-head attention mechanisms in transformer models [26], we fuse c branches individually and aggregate the results by taking the sum, as shown in Figure 3. We define the message functions as

$$M_{\mathcal{O} \rightarrow \mathcal{H}}(\mathbf{y}_j^t, \mathbf{z}_{ij}) = \text{MultiBranchFusion}_o(\mathbf{y}_j^t, \mathbf{z}_{ij}) \quad (5)$$

$$M_{\mathcal{H} \rightarrow \mathcal{O}}(\mathbf{x}_i^t, \mathbf{z}_{ij}) = \text{MultiBranchFusion}_h(\mathbf{x}_i^t, \mathbf{z}_{ij}). \quad (6)$$

Importantly, the two fusion modules do not share weights. This allows the learned spatial attention to be conditioned on the message passing direction, and the mapped appearance features to be tailored to the nature of their senders, i.e., human or object nodes.

We also use spatial information to modulate the appearance features when computing the adjacency matrix. Since the representation size of the spatial fusion head is n , we employ an additional linear layer to map it to a scalar. The pre-normalized adjacency is computed as

$$\tilde{\alpha}_k = \mathbf{w}_k^T \sigma(\text{MultiBranchFusion}_\alpha(\mathbf{x}_i^t \oplus \mathbf{y}_j^t, \mathbf{z}_{ij})) + b_k \quad (7)$$

where $\mathbf{w}_k \in \mathbb{R}^n$, $b_k \in \mathbb{R}$ and k is a linear index corresponding to a pair of (i, j) , that is, $k \in \{1, \dots, |\mathcal{H}| \times |\mathcal{O}|\}$. During message passing, the adjacency value α_{ij} is obtained by applying softmax to the entries sharing the same index i . Similarly, α_{ji} is normalized by fixing j .

After all iterations of message passing, we fuse the spatial features and the refined graph features prior to binary classification for each target class. The computation of pre-sigmoid logits has the same form as that of the adjacency matrix in (7), except that the output dimension is equal to the number of target classes. In fact, the adjacency can be interpreted as general interactiveness while the class probabilities are further conditioned on action types. For this reason the two multi-branch fusion modules share weights, which reduces the number of parameters and speeds up the training process.

3.3. Global Cues

As with most RoIPool-based feature extraction methods, the pooled information is local to an area. While this is reasonable for object detection, longer-range information about the global scene can be crucial for understanding human-object interactions. To this end, we employ another multi-branch fusion module and fuse the global features extracted from the backbone with the spatial features for each pair of nodes. The resultant features are concatenated with the graph features for final classification.

3.4. Training and Inference

For each image, we append ground-truth boxes with a score of one to the set of detections during training. Then we remove detected boxes below a particular score and apply non-maximum suppression. Among the remaining detections, the m highest scoring human and object boxes are selected to initialize the bipartite graph. After message passing, we generate a set of human–object pairs from the graph, denoted by $\{q_k\}_{k=1}^{|\mathcal{H} \times \mathcal{O}|}$, where $q_k = (\mathbf{b}_i^h, \mathbf{b}_j^o, \tilde{\mathbf{s}}_k)$. The bounding boxes \mathbf{b} are obtained from the corresponding human and object nodes connected by edge (i, j) . The post-sigmoid classification scores for all actions $\tilde{\mathbf{s}}_k$ are multiplied by the object detections scores to give the final scores

$$\mathbf{s}_k = s_i^h \cdot s_j^o \cdot \tilde{\mathbf{s}}_k. \quad (8)$$

To associate the detected human–object pairs with ground-truth, the intersection-over-union is computed between each detected pair and ground-truth pair. Following previous practice [3], the IoU is computed for human and object boxes separately and taken as the minimum of the two. Detected pairs are considered as positive when the IoU is above a designated threshold.

Due to the nature of proposal generation, there are overwhelmingly more negative examples than positive ones. In particular, easy negatives compose the majority. This inhibits the model from further improving on examples that are not well classified. To alleviate this issue, we adopt the focal loss [17] as a binary classification loss, given by

$$\text{FL}(\hat{y}, y) = \begin{cases} -\beta(1 - \hat{y})^\gamma \log(\hat{y}), & y = 1 \\ -(1 - \beta) \hat{y}^\gamma \log(1 - \hat{y}), & y = 0 \end{cases} \quad (9)$$

where $\hat{y} \in [0, 1]$ is the final score of an example for a certain class, $y \in \{0, 1\}$ is the binary label, and $\beta \in [0, 1]$ and $\gamma \in \mathbb{R}_+$ are hyper-parameters. In particular, β is a balancing factor between positive and negative examples. With $\beta > 0.5$, positive examples are assigned higher weights and vice versa. The parameter γ attenuates the loss incurred on well-classified examples. This prevents the large number of easy negatives from dominating the gradient. However, suppressing easy negatives reduces the focal loss’ magnitude [17], and so normalization is required. We extend Lin et al.’s [17] proposal to binary classification by normalizing the loss by the number of positive logits.

Another important aspect is the correspondence between the predicted actions and target interactions. Suppose the set of actions is denoted by \mathcal{A} . Furthermore, for a specific object type $o \in \mathcal{K}$, denote the subset of valid actions as \mathcal{A}_o . The interactions of interest can be represented as the set $\mathcal{I} = \cup_{o \in \mathcal{K}} \mathcal{A}_o \times \{o\}$, with $\mathcal{I} \subseteq \mathcal{A} \times \mathcal{K}$. Following the practice of Gupta et al. [10], we only compute the loss on the subset of actions \mathcal{A}_o for each human–object pair, given

the object type o . This process removes predictions on non-existent interaction types, for instance, *eating a car*. Therefore, the network parameters can be dedicated to learning other meaningful interactions.

In the HICO-DET dataset [3], interactions of interest include those between two humans (i.e., a human may be an object and a subject in an HOI triplet). To capture such interactions, we construct bipartite graphs such that object nodes subsume human nodes, that is, object nodes are identical to the set of all detections. Human nodes representing the same instance across the bipartition are initialized to be the same, yet will diverge as message passing proceeds.

4. Experiments

4.1. Dataset and Metric

We conducted our experiments on the large scale HOI detection dataset HICO-DET [3]. It contains 38 118 training and 9 658 test images. The dataset is an extension of its predecessor HICO [4], which contains image-level annotations of human–object interactions. Due to the fact that some of these interactions cannot be localized in the form of human–object pairs, a small proportion of images are left with image-level labels only. These images are discarded during both training and testing, following the protocol established by Chao et al. [3]. In total, there are 37 633 training and 9 546 test images with bounding box annotations. There are 80 object classes, identical to those in the MS COCO dataset [19], 117 action types, and 600 interaction types. In terms of samples, there are 117 871 annotated human–object pairs in the training set and 33 405 in the test set. The distribution of pairs per interaction class is highly uneven, following a long tail distribution. In particular, there are 47 interaction categories with only one training example.

To capture the effectiveness of our model across interactions with different numbers of annotations, we follow previous practice and report on three categories: 600 interactions (full), 138 interactions with fewer than 10 training examples (rare) and 462 interactions with 10 or more training examples (non-rare). Mean average precision (mAP) is used as the evaluation metric. Detected human–object pairs are considered as positive when the IoU with any ground-truth pair is higher than 0.5. For multiple detected pairs associated with the same ground-truth instance, only the highest scoring pair is considered as positive. The computation of mAP follows the 11-point interpolation algorithm used in Pascal VOC challenge [5].

4.2. Implementation Details

Prior to training, we employ Faster R-CNN [23] with ResNet50-FPN [13, 18] pretrained on MS COCO [19] to generate detections. For each image, we first filter out

detections with scores lower than 0.5 and perform non-maximum suppression (NMS) with a threshold of 0.5. Afterwards, we extract the $m = 10$ highest scoring human boxes, and the $m = 10$ highest scoring object boxes. This gives us at most $10(20 - 1) = 190$ box pairs, with pairs involving the same person twice having been removed. Inference follows the same setup, except that ground-truth detections are not used.

We use ResNet50-FPN [13, 18] as the backbone for feature extraction. The backbone parameters are fixed during training. To utilize the feature pyramid, boxes are assigned to different pyramid levels based on their sizes [18]. The pooled box features are mapped to 1024-dimensional vectors with a two-layer MLP. Similarly, the spatial features are mapped to the same dimension (1024) with a three-layer MLP. For the multi-branch fusion head, we use $c = 16$ and $n = 1024$. We use two iterations of message passing for all models. To augment the object detection scores, we use low-grade instance suppression (LIS) as proposed by Li et al. [15]. Lastly, for the focal loss, we set the hyperparameters as $\beta = 0.5$ and $\gamma = 0.5$.

We adopt an image-centric training strategy [8] with slight modifications. Input images are normalized and resized such that the shorter edge is 800 pixels. Bounding boxes are then resized accordingly. Afterwards, images are batched with zero padding. We use a batch size of 4. To train the model, we use stochastic gradient descent as the optimizer, with a momentum of 0.9 and weight decay of 10^{-4} . We use an initial learning rate of 10^{-3} and decrease it to 10^{-4} at the tenth epoch. All models are trained for 15 epochs on a single GeForce GTX TITAN X device. The full model takes 48 hours to train.

4.3. Comparison with State-of-the-Art

Quantitative results on the HICO-DET [3] test set are shown in Tab. 1. We report the performance of our model separately using a detector pre-trained on the MS COCO dataset [19], a detector fine-tuned on HICO-DET and the ground truth detections. We achieve competitive performance when using the COCO pre-trained detector compared to methods with a similar lightweight backbone, but significantly outperform state-of-the-art when using the cleaner fine-tuned detections, a 10% relative improvement. In particular, we outperform the next best method, DRG [6], by 2.65 mAP, despite underperforming that method by 1 mAP when using the COCO detections. This suggests that our graph neural network can better exploit the high-quality detections. Further evidence supporting this argument can be seen from using the ground truth object locations where we are able to outperform previous best method (also using ground truth detections) by 40% in relative terms. We show an example of the different detector outputs in Fig. 4. Less salient people and objects are suppressed in the fine-tuned

Table 1. Detection results (mAP $\times 100$) on the HICO-DET [3] test set. Methods in the top section use an object detector pre-trained on MS COCO [19], methods in the middle section are trained end-to-end or use an object detector fine-tuned on HICO-DET, and methods in the bottom section use ground truth detections.

Method	Backbone	Full	Rare	Non-rare
(MS COCO DETECTIONS)				
HO-RCNN [3]	CaffeNet	7.81	5.37	8.54
InteractNet [9]	ResNet-50-FPN	9.94	7.16	10.77
GPNN [22]	ResNet-101	13.11	9.34	14.23
iCAN [7]	ResNet-50	14.84	10.45	16.15
Wang et al. [28]	ResNet-50	16.24	11.16	17.75
Bansal et al. [2]	ResNet-101	16.96	11.73	18.52
RP _D C _D [15]	ResNet-50	17.03	13.42	18.11
RP _{T2} C _D [15]	ResNet-50	17.22	13.51	18.32
Gupta et al. [10]	ResNet-152	17.18	12.17	18.68
RPNN [31]	ResNet-50	17.35	12.78	18.71
PMFNet [27]	ResNet-50-FPN	17.46	15.65	18.00
Wang et al. [11]	ResNet-50-FPN	17.57	16.85	17.78
DRG [6]	ResNet-50-FPN	19.26	17.74	19.71
Peyre et al. [21]	ResNet-50-FPN	19.40	14.63	20.87
VSGNet [25]	ResNet-152	19.80	16.05	20.91
Ours	ResNet-50-FPN	18.26	13.40	19.71
(HICO-DET DETECTIONS)				
PPDM [16]	DLA-34	20.29	13.06	22.45
PPDM [16]	Hourglass-104	21.73	13.78	24.10
Bansal et al. [2]	ResNet-101	21.96	16.43	23.63
DRG [6]	ResNet-50-FPN	24.53	19.47	26.04
Ours	ResNet-50-FPN	27.18	19.41	29.50
(GROUND TRUTH DETECTIONS)				
iCAN [7]	ResNet-50	33.38	21.43	36.95
Peyre et al. [21]	ResNet-50-FPN	34.35	27.57	36.38
Ours	ResNet-50-FPN	47.88	34.03	52.01



Figure 4. Object detections from the pre-trained MS COCO model (left) compared to the fine-tuned HICO-DET model (right). Boxes with scores higher than 0.5 are displayed. The fine-tuned detector suppresses objects that are less likely to be engaged in interactions.

detector.

Qualitative results are presented in Fig. 5. We also compare our baseline and full models in Fig. 6, showing that modulating the appearance features with spatial information allows our model to more accurately infer the correspondences between humans and objects. This is particularly helpful for images with many prominent human and object instances. We also show some failure cases in Fig. 7. In particular, human-object pairs with plausibly-related spa-

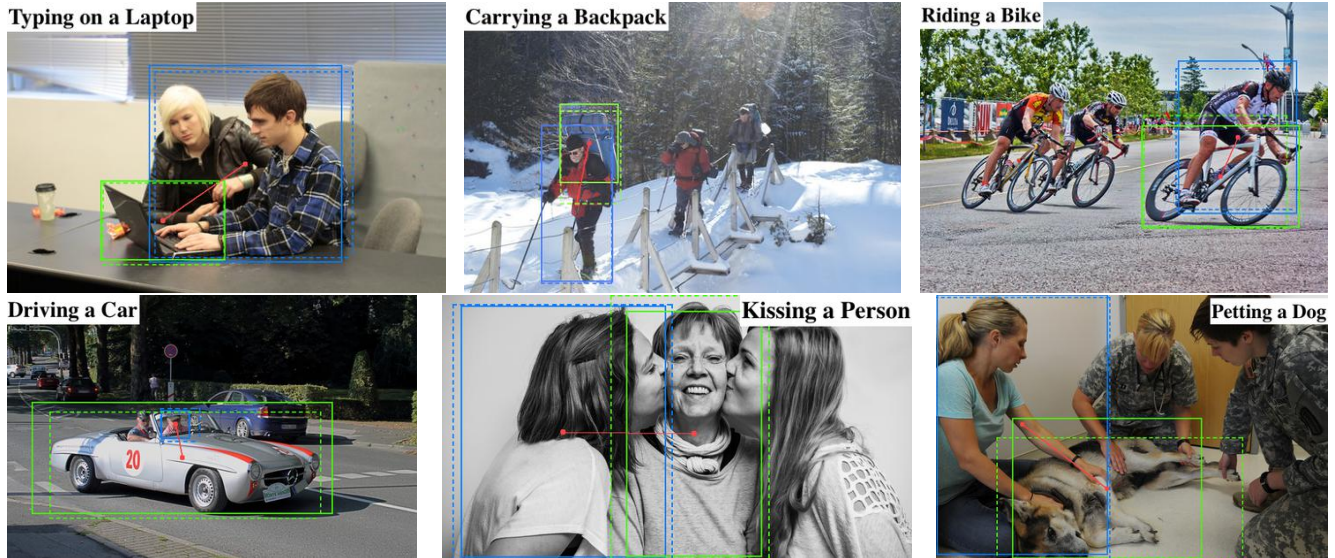


Figure 5. Qualitative results. We visualize detected human–object pairs with solid bounding boxes, with the human in a blue box and the object in a green box. The associated ground-truth box pair is shown with dashed lines.

Table 2. Injecting spatial information at different locations. We denote the computation of the adjacency matrix as A , message passing as M , global features as G and refined graph features as R .

Model	COCO Detector	HICO-DET Detector
Baseline	17.06	24.47 (+7.41)
Baseline + A	17.01	25.80 (+8.79)
Baseline + M	17.66	26.42 (+8.76)
Baseline + G	17.59	26.47 (+8.88)
Baseline + R	17.64	26.55 (+8.91)
Baseline + A, M, R	17.84	26.69 (+8.85)
Baseline + A, M, R, G	18.26	27.18 (+8.92)

Table 3. Varying the number of branches in multi-branch fusion.

Model	COCO Detector	HICO-DET Detector
Ours $c = 1$	17.61	26.27 (+8.66)
Ours $c = 8$	17.92	26.83 (+8.91)
Ours $c = 16$	18.26	27.18 (+8.92)

Table 4. Comparison between different loss functions: binary cross-entropy (BCE) and focal loss (FL).

Model	COCO Detector	HICO-DET Detector
Baseline w/ BCE	15.73	23.33 (+7.60)
Baseline w/ FL	17.06	24.47 (+7.41)
Ours w/ BCE	17.84	26.29 (+8.45)
Ours w/ FL	18.26	27.18 (+8.92)

tial configurations seem to confuse our model.

4.4. Ablation Studies

We conducted a series of ablation studies to demonstrate what contributes most to the effectiveness of our model.

Table 5. Varying the number of message passing iterations

Model	COCO Detector	HICO-DET Detector
Ours w/ 0 iter.	17.49	26.52(+9.02)
Ours w/ 1 iter.	17.95	26.88(+8.93)
Ours w/ 2 iter.	18.26	27.18(+8.92)
Ours w/ 3 iter.	17.95	26.89(+8.94)

Our baseline is a bipartite graph with appearance features only. Specifically, the message sent from a node is computed from its appearance encodings using a linear layer. The adjacency and class probabilities are computed from the concatenated node encodings of a human–object pair using an MLP, and the computation shares weights until the logistic layer. We first investigate the importance of injecting spatial information at all of the locations used in our model: for computing the adjacencies (A), messages (M), global features (G) and refined graph features (R). As shown in Tab. 2, every location improves over the baseline, and they combine together to achieve the best performance (the final row is equivalent to our full model). We next demonstrate the benefit of using multiple branches to fuse the spatial and appearance information. As shown in Tab. 3, the performance improves with the number of branches (cardinality). We also show, in Tab. 4, that there is some benefit to adopting the focal loss for this task, suggesting that it is useful for attenuating the influence of the extremely large number of easy negatives. Lastly, we show how the number of message passing iterations at test time affects the results. As shown in Tab. 5, message passing is clearly helpful for this problem (comparing rows 1 and 2), while an additional iteration further improves the results.



Figure 6. Comparison of the baseline model (without spatial information) and the full model (with spatial information). False positive HOI detections for a particular action type are shown, alongside their scores from the baseline model (B) and full model (F). Detected box pairs are shown with solid lines while the ground-truth box pair with the highest IoU is shown with dashed lines. In these examples, the spatial cues strongly indicate that the putative human-object pairs do not correspond to the given action. Unlike the baseline, our full model uses this information to suppress the false positives, assigning them a low score.



Figure 7. Failure cases with predicted action and score. Spatial configurations that are plausible for a given action can confuse the model.

5. Conclusion

In this paper, we have proposed a spatio-attentive graph neural network for detecting human–object interactions. To exploit the appearance and spatial features jointly, we introduced a multi-branch fusion mechanism that modulates the appearance features with the spatial configuration of the human–object pairs. We applied this mechanism in the computation of the adjacency structure, graph messages, global features and refined graph features, and show that our model outperforms the state-of-the-art by a considerable margin.

References

- [1] Lei Jimmy Ba, Jamie Ryan Kiros, and Geoffrey E. Hinton. Layer normalization. *Adv. Neural Inform. Process. Syst.*, 2016. 4
- [2] Ankan Bansal, Sai Saketh Rambhatla, Abhinav Shrivastava, and Rama Chellappa. Detecting human-object interactions via functional generalization. *AAAI*, 2020. 6
- [3] Yu-Wei Chao, Yunfan Liu, Xieyang Liu, Huayi Zeng, and Jia Deng. Learning to detect human-object interactions. *Proceedings of the IEEE Winter Conference on Applications of Computer Vision*, 2018. 1, 2, 5, 6
- [4] Yu-Wei Chao, Zhan Wang, Yugeng He, Jiaxuan Wang, and Jia Deng. HICO: A benchmark for recognizing human-object interactions in images. *Int. Conf. Comput. Vis.*, 2015. 5
- [5] Mark Everingham, S. M. Ali Eslami, Luc Van Gool, Christopher K. I. Williams, John Winn, and Andrew Zisserman. The Pascal visual object classes challenge: A retrospective. *Int. J. Comput. Vis.*, 111(1):98–136, 2014. 5
- [6] Chen Gao, Jiarui Xu, Yuliang Zou, and Jia-Bin Huang. DRG: Dual relation graph for human-object interaction detection. *Eur. Conf. Comput. Vis.*, 2020. 1, 2, 3, 6
- [7] Chen Gao, Yuliang Zou, and Jia-Bin Huang. iCAN: Instance-centric attention network for human-object interaction detection. *Brit. Mach. Vis. Conf.*, 2018. 1, 2, 6
- [8] Ross Girshick. Fast R-CNN. *Int. Conf. Comput. Vis.*, (9):1440–1448, 2015. 2, 6
- [9] Georgia Gkioxari, Ross Girshick, Piotr Dollár, and Kaiming He. Detecting and recognizing human-object interactions. *IEEE Conf. Comput. Vis. Pattern Recog.*, 2018. 6
- [10] Tanmay Gupta, Alexander Schwing, and Derek Hoiem. No-frills human-object interaction detection: Factorization, layout encodings, and training techniques. *Int. Conf. Comput. Vis.*, 2019. 1, 2, 4, 5, 6
- [11] Wang Hai, Zheng Weishi, and Yingbiao Ling. Contextual heterogeneous graph network for human-object interaction detection. *Eur. Conf. Comput. Vis.*, 2020. 1, 2, 3, 6
- [12] Kaiming He, Georgia Gkioxari, Piotr Dollár, and Ross Girshick. Mask R-CNN. *Int. Conf. Comput. Vis.*, pages 2980–2988, 2017. 2, 3
- [13] Kaiming He, Xiangyu Zhang, Shaoqing Ren, and Jian Sun. Deep residual learning for image recognition. *IEEE Conf. Comput. Vis. Pattern Recog.*, pages 770–778, 2016. 5, 6
- [14] Hei Law and Jia Deng. CornerNet: Detecting objects as paired keypoints. *Eur. Conf. Comput. Vis.*, 2018. 2
- [15] Yong-Lu Li, Siyuan Zhou, Xijie Huang, Liang Xu, Ze Ma, Hao-Shu Fang, Yanfeng Wang, and Cewu Lu. Transferable interactiveness knowledge for human-object interaction detection. *Int. Conf. Comput. Vis.*, 2019. 1, 2, 6
- [16] Yue Liao, Si Liu, Fei Wang, Yanjie Chen, Chen Qian, and Jiashi Feng. PPDM: Parallel point detection and matching for real-time human-object interaction detection. *IEEE Conf. Comput. Vis. Pattern Recog.*, 2020. 2, 6
- [17] Tsung-Yi Lin, Priya Goyal, Ross B. Girshick, Kaiming He, and Piotr Dollár. Focal loss for dense object detection. *Int. Conf. Comput. Vis.*, 2017. 5
- [18] Tsung-Yi Lin, Piotr Dollár, Ross Girshick, Kaiming He, Bharath Hariharan, and Serge Belongie. Feature pyramid networks for object detection. *IEEE Conf. Comput. Vis. Pattern Recog.*, 2017. 5, 6
- [19] Tsung-Yi Lin, Michael Maire, Serge Belongie, James Hays, Pietro Perona, Deva Ramanan, Piotr Dollár, and C. Lawrence Zitnick. Microsoft COCO: Common objects in context. *Eur. Conf. Comput. Vis.*, 2014. 5, 6
- [20] Cewu Lu, Ranjay Krishna, Michael Bernstein, and Li Fei-Fei. Visual relationship detection with language priors. *Eur. Conf. Comput. Vis.*, 2016. 1
- [21] Julia Peyre, Ivan Laptev, Cordelia Schmid, and Josef Sivic. Detecting unseen visual relations using analogies. *Int. Conf. Comput. Vis.*, 2019. 1, 2, 6
- [22] Siyuan Qi, Wenguan Wang, Baoxiong Jia, Jianbing Shen, and Song-Chun Zhu. Learning human-object interactions by graph parsing neural networks. *Eur. Conf. Comput. Vis.*, 2018. 1, 2, 6
- [23] Shaoqing Ren, Kaiming He, Ross B. Girshick, and Jian Sun. Faster R-CNN: Towards real-time object detection with region proposal networks. *Adv. Neural Inform. Process. Syst.*, pages 91–99, 2015. 1, 2, 3, 5
- [24] Olga Russakovsky, Jia Deng, Hao Su, Jonathan Krause, Sanjeev Satheesh, Sean Ma, Zhiheng Huang, Andrej Karpathy, Aditya Khosla, Michael Bernstein, Alexander C. Berg, and Li Fei-Fei. ImageNet large scale visual recognition challenge. *Int. J. Comput. Vis.*, 115(3):211–252, 2015. 1
- [25] Oytun Ulutan, A S M Iftekhhar, and B. S. Manjunath. VS-GNet: Spatial attention network for detecting human object interactions using graph convolutions. *IEEE Conf. Comput. Vis. Pattern Recog.*, 2020. 1, 2, 3, 6
- [26] Ashish Vaswani, Noam Shazeer, Niki Parmar, Jakob Uszkoreit, Llion Jones, Aidan N Gomez, Łukasz Kaiser, and Illia Polosukhin. Attention is all you need. *Adv. Neural Inform. Process. Syst.*, 30:5998–6008, 2017. 4
- [27] Bo Wan, Desen Zhou, Yongfei Liu, Rongjie Li, and Xuming He. Pose-aware multi-level feature network for human object interaction detection. *Int. Conf. Comput. Vis.*, 2019. 2, 6
- [28] Tiancai Wang, Rao Muhammad Anwer, Muhammad Haris Khan, Fahad Shahbaz Khan, Yanwei Pang, Ling Shao, and Jorma Laaksonen. Deep contextual attention for human-object interaction detection. *Int. Conf. Comput. Vis.*, 2019. 6

- [29] Saining Xie, Ross B. Girshick, Piotr Dollár, Zhuowen Tu, and Kaiming He. Aggregated residual transformations for deep neural networks. *IEEE Conf. Comput. Vis. Pattern Recog.*, pages 5987–5995, 2017. [4](#)
- [30] Bolei Zhou, Agata Lapedriza, Aditya Khosla, Aude Oliva, and Antonio Torralba. Places: A 10 million image database for scene recognition. *IEEE Trans. Pattern Anal. Mach. Intell.*, 2017. [1](#)
- [31] Penghao Zhou and Mingmin Chi. Relation parsing neural network for human-object interaction detection. *Int. Conf. Comput. Vis.*, 2019. [2](#), [3](#), [6](#)